Published by Avanti Publishers

Journal of Advanced Thermal Science Research

ISSN (online): 2409-5826

Journal of Advanced Thermal Science Research

Cooling Strategy Optimization of a Permanent Magnet Synchronous Motor

Mert Bedirhan Genç[1], Rami Habash[2], Gamze Gediz Ilis[1,*], Alkan Alkaya[3], Hakan F. Öztop[4]

[1]*Department of Mechanical Engineering, Gebze Technical University, Gebze, Turkey*
[2]*Department of Mechanical Engineering, Istanbul Okan University, Istanbul, Turkey*
[3]*Department of Electrical and Electronics Engineering, Mersin University, Mersin, Turkey*
[4]*Faculty of Technology, Department of Mechanical Engineering, Firat University, Elazig, Turkey*

ARTICLE INFO

Article Type: Research Article

Academic Editor: Glauber Cruz

Keywords:
CFD
Taguchi method
Thermal analysis
Cooling of motor
Permanent magnet synchronous motor

Timeline:
Received: October 06, 2023
Accepted: December 02, 2023
Published: December 22, 2023

Citation: Genç MB, Habash R, Ilis GG, Alkaya A, Öztop HF. Cooling strategy optimization of a permanent magnet synchronous motor. J Adv Therm Sci Res. 2023; 10: 75-88.

DOI: https://doi.org/10.15377/2409-5826.2023.10.6

ABSTRACT

In this study, 250 kW, 9 phase, outer rotor types of Permanent Magnet Synchronous Motor (PMSM) are taken into consideration. To optimize the cooling efficiency of the motor, firstly, the motor geometry is obtained, and the e-magnetic model of the geometry is validated with the manufacturer`s data. Secondly, by using the validated e-magnetic model, the cooling system of the motor was analyzed by using the thermal model of the Motor-CAD. The thermal model is also validated with the real-time experiments which are held on an electric bus at constant speed experimentally. For finding the best cooling strategy for the motor, after validation, the effect of the mass flow rate, the type of the cooling refrigerant, the cooling pipe diameter size, and the change of torque are analyzed on the validated model. The results showed us that mass flow rate and torque have a significant effect on winding temperature, and the Taguchi method showed that [mass flow rate (A)=50 l/min, pipe diameter (B) = 17.7 mm, number of turns (C)=20, type of fluid (D)= EGW50/50, torque (E)=2000 Nm] is the best cooling design parameters for the cooling strategy of the considered PMSM.

*Corresponding Author
Emails: ggediz@gtu.edu.tr; ggedizilis@gmail.com
Tel: +(90) 262 605 10 00

1. Introduction

Transportation is one of the most elementary needs of the population. Efforts to respond to this fundamental need are growing with the development of technology. Due to the growing interest in electric vehicles over the past few years, automotive technology is concentrating on this area. Although electric vehicles have been on the agenda for several years, the earliest examples date back to the 1800s. However, in those years, reasons such as inadequate battery technology have diminished interest in electric vehicles.

Today, electric vehicles have reappeared for reasons such as the reduction in demand for oil, and thus, environmental pollution and the millage problems which have been overcome by increasing electric vehicle usage. Transportation in the world is one of the main reasons for CO_2 emissions, which pushes manufacturers to come up with a new technology to replace the traditional internal combustion engine with an electric one. According to a European Union report, the transportation sector is responsible for almost 28 % of total carbon dioxide (CO_2) emissions, while road transport is accountable for over 70 % of the transport sector emissions [1].

The Permanent Magnet Synchronous Motor (PMSM) attracted the attention of the electric automotive industry because of its high power, high efficiency, torque density, and reliability [2]. Due to high internal heat generation in PMSM, the power density, longevity, and reliability are reduced [3].

Therefore, advanced heat management becomes a necessary condition for the improvement of power capacity and torque density. Thermal analysis of electrical machines has not been sufficiently studied. The importance of this problem increases significantly due to cost-saving and an increase in energy-efficiency requirements. The need for high-thermal-performance motors is important due to the increase in electric vehicle applications [4]. Regarding cooling methods, various systems have been developed related to the operating fluid, cooling strategy, and thus motor performance [5]. Many techniques are used such as air-cooling [6], oil-cooling [7], liquid cooling [8], and hydro-cooling systems [9] for the improvement of motor performance. A liquid-cooling system such as an air-cooling system works on taking away the generated heat from the winding of the motor, but in this method, it uses the circulating flow of the coolant over it. The liquid-cooling system meets the cooling and heating conditions requirements of the motor more easily than the air system does, and this is due to specific heat capacity. In addition to the type of cooling system, other parameters, such as the flow rate of the fluid, its inlet temperature, and the choice of the appropriate coolant for each case must be important for the overall thermal performance of the cooling system and the thermal behavior of the motor.

For a high-power density in an electrical motor, air cooling becomes insufficient, and liquid cooling starts to be used for high-capacity motors [10]. Rehman *et al*. [11] numerically studied the thermal performance of a water-cooled induction motor at a constant thermal load. In this study, the optimum number of coolant flow passes is also specified. Cavazzuti *et al*. [12] studied the conduction resistance between stator teeth and water jackets by developing the Lumped Parameter Thermal Network (LPTN) model for water-cooled PMSM. The winding, stator, rotor, and magnet properties are temperature-dependent, and due to that; the electromagnetic losses of the motor are coupled with the thermal characteristics. Zhan *et al*. [13] predicted the electromagnetic losses and temperature distribution accurately by developing a 3D electromagnetic and thermal model. In this study, the numerical and the experimental measurements are compared, and a new ventilation design is suggested to have good temperature distribution. Lundmark *et al*. [14] studied the electromagnetic and thermal performance of an internal water jacket-cooled permanent magnet motor by using ANSYS. The results showed that the interior permanent magnet transverse flux motor cooling is very efficient due to the lack of end winding. Aziz and Atkinson [15] studied two types of thermal modeling methods to predict the temperature of a PMSM. The predicted temperature from the lumped parameter model and finite element analysis are compared, and the results were validated by experiment setup. Results showed that both thermal analysis methods give the same results and show the rise of temperature on each part of the machine. The study which was conducted by Demetriades, *et al*. [16] presents a real-time thermal model with calculated parameters based on the geometry of the different components of a permanent-magnet synchronous motor. Simulation results were compared with experimental results to study the performance and the feasibility of the concept. Ponomarev *et al*. [17] built three models, the lumped parameters (LPTN), the thermostatic FEM model, and the Computational fluid dynamic (CFD)

model. This paper studies the potential and effectiveness of direct oil cooling of a PMSM. the CFD model allows precise determination of the cooling prospects, which gives the required information to choose the optimal volumetric coolant flow. Johnston *et al*. [18] studied numerically the overall effectiveness of four different cooling technologies, the results showed that the direct winding heat exchanger technology has better electrothermal performance compared to the other technologies. Fan *et al*. [19] analyzed the thermal behavior of the driving motor by applying the lumped thermal parameter method, and the temperature distribution in the drive motor was estimated under the actual driving duty cycle. A test bench is built to measure the temperature distribution, and the results of these calculations are compared and discussed with the experimental results. Fang *et al*. [20] study the cooling strategy of PMSM. Two thermal management with different heat-pipe layouts are created. The effect of the ambient temperature and various operating conditions for two different models are analyzed. The results of the experimental and simulation studies show that the use of SEME promotes higher heat dissipation ability than RM. Sun *et al*. [21] studied the permanent magnet manufactured by encapsulating potting silicone gelatin (P-M) between the end windings and the motor casing to a liquid cooling PMSM(O-M). The three-dimensional model of PMSM was created, and the temperature rise performances under different operating conditions were compared with the O-M to measure the heat dissipation enhancement. The temperatures of the cooling fluid are compared when the motor works under different velocity and torque values.

As summarized in Fig. (**1**), most of the studies taken into account in the literature on the synchronous motor are performed for low power scales [4, 11, 12, 15-47]. After a detailed literature survey, limited studies are found for high motor powers such as above 200 kW. Due to limited studies on high-power motors, this paper is focused on a 250 kW power PMSM which is one of the most important differences between the studies found in the literature.

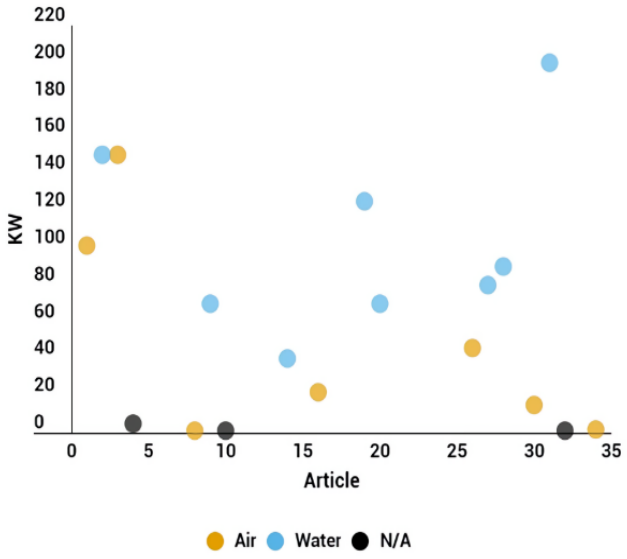

Figure 1: Air and water cooling studied article numbers.

Limited studies are focusing on the cooling pipe system, as mentioned above literature. Thus, this study is focused on a novel designed permanent magnet synchronous motor which is 250 kW and 9 phases. This motor is taken into account due to its high capacity and its unique cooling pipe location which is inside the motor. The main originality of the work is that the chosen motor has a cooling pipe on the stator side and thus this design causes us to make limited changes in cooling design. All of them deal with the cooling pipe system which is located on the jacket of the synchronous motor. The motor, which is cooled by the refrigerant fluid over the parallel fixed channels on the fixed stator, has a single-phase flow in cooling pipes. In this study, the data of the motor is provided from the motor company manual and taken as a reference. The motor geometry is generated, and both the e-magnetic and thermal models of the motor are validated with the manufacturer's manual data. After validation of this paper, the authors focused on the cooling systems of the motor, the mass flow rate of the refrigerant, the type of the cooling refrigerant, and the cooling pipe diameter size are analyzed. The critical

parameters that affect the temperature profile are identified in this study. Understanding the effect of the parameters on the temperature distribution helps us to develop the best cooling design which achieves the best efficiency and performance.

2. The Geometry of the Motor

The PMSM which is taken into account is 250 kW and has an outer rotor topology [48]. The rotor structure includes the cooling pipe system which is fixed on the stator. The generated heat from the motor is removed by circulating the coolant in a pipe that has a diameter of 1-inch diameter. The cooling pipe is located on the winding area of the stator where most of the heat is generated. The total length of the cooling-fluid pipe is 4540 mm and has 12 passes on the stator. Table **1** shows the geometrical parameters, and the material details of the PMSM, respectively. Fig. (**2**) shows the three-dimensional geometry of the considered PMSM and presents the view of the cooling pipes on the stator. The cooling jacket is placed on a stator that is close to the winding. The 60/40 EWG (Water/Ethylene Glycol) water flows inside the pipes for cooling the motor. The thermophysical properties of the materials that are used to construct the considered motor are given in Table **2** (from the library of MotorCAD).

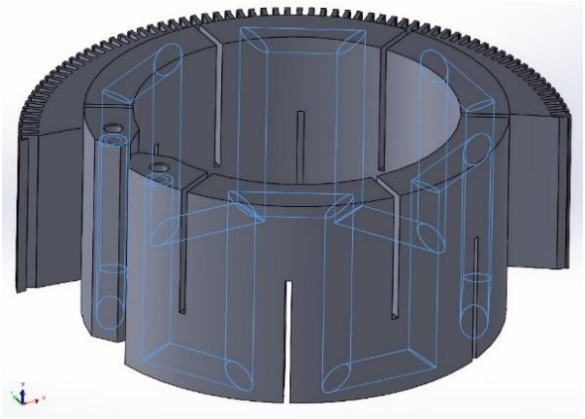

Figure 2: Motor cooling pipe on stator volume.

Table 1: Main parameters of motor.

Parameters	Value
Slot/Pole Number	16
Slot Number	144
Axle Dia [mm]	340
Motor Lenght [mm]	511
Stator Lam Lenght [mm]	188

Table 2: The thermophysical parameters of the material.

Part of the Motor	Material	Thermal Conductivity (W/mK)
Rotor	Aluminum alloy	168
Stator	Steel	30
Insulation	Epoxy	0.22
Winding	Copper	401

3. Governing Equations

To study the thermal behavior of the motor, three elements are required to be studied: heat transfer, heat storage, and heat generation of the motor. The heat storage and heat transfer are modeled by the thermal resistance and thermal capacitance method, and the heat generation is obtained by studying the generated losses. The heat conduction equation for the motor can be written as [49]:

$$\rho c_s \frac{\partial T}{\partial t} = p + div(\lambda \nabla(T)) \tag{1}$$

Thermal resistance and thermal capacitance can be written as [49]:

$$R_{cond} = \frac{l}{\lambda S} \tag{2}$$

$$C = C_p \rho V \tag{3}$$

Also, the losses of the motor (copper and iron losses) are the most important parameters that affect the thermal distribution of the motor. The losses can be classified into three categories such as copper losses, iron losses in the teeth, and iron losses in the stator yoke. These losses can be defined as follows [49]:

Copper losses:

$$Pj = 3R_{ph}I_{eff}2 = 3R_{ph}\left(\frac{i_{max}}{\sqrt{2}}\right) \tag{4}$$

R_{ph} is the phase resistance and can be given by the following expression [50]:

$$R_{ph} = R_{cu}(T_{cu})\frac{N_{sph}L_{sp}}{S_c} \tag{5}$$

Iron losses in the teeth and the stator yoke can be written as [50]:

$$P_{f-d} = q\left(\frac{f}{50}\right)^{1.5}[M_{ds}{B_d}^2] \tag{6}$$

$$\mathrm{P_{f-c}} = \mathrm{q}\left(\frac{\mathrm{f}}{50}\right)^{1.5}[\mathrm{M_{cs}}{\mathrm{B_c}}^2] \tag{7}$$

4. Validation of the Developed Model

4.1. E-Magnetic Model

A magnetic model must be created before the thermal model. The magnetic model provides the power, torque, and velocity values. All results from the magnetic model directly or indirectly affect the losses because the geometrical parameters create the losses. Because of that, the design parameters are the biggest variables that affect the losses. Especially the winding around is the region where the losses are most densely. The slot type and the slot area define the motor power and its efficiency, while the winding type and the winding dimensions affect the power and the efficiency.

According to the literature, the air convection velocity over the motor, the ambient temperature, the coolant velocity, the gap of the casing, the thickness of the stator core, and the thickness of the slot insulation are the factors that affect the temperature rise of the motor. Thus, the design of the motor itself is the main consideration for the temperature rise. To analyze the thermal performance of the motor, the thermal model is simulated by Motor-CAD, and the results are studied in this study.

The torque and speed values obtained from the e-magnetic Motor-Cad model of the 250 kW PMSM are compared with the technical data which is given by the manufacturer of this motor, and the comparison for 750 Vdc and 600Vdc values is illustrated in Fig. (**3**). As seen, the e-magnetic model which is developed in this study has the best fit with the technical specs of the manufacturers.

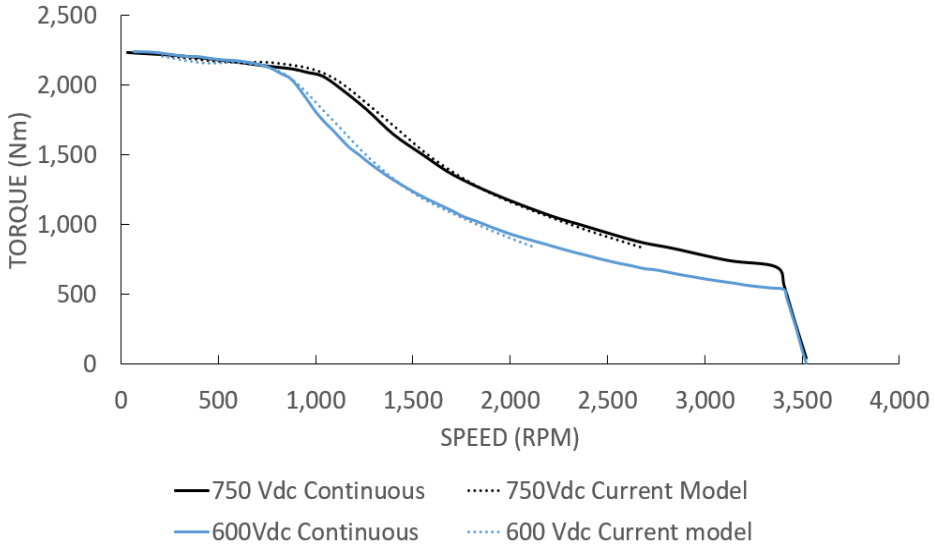

Figure 3: The validation results of the e-magnetic model.

4.2. Thermal Model

After validation of the e-magnetic model of PMSM, the thermal model of the PMSM is taken into account. The parameters that are used to validate the thermal model of the motor are summarized in Table **2**. By using the parameters given in Table **2**, the thermal model is validated with an experimental result. The experiment is performed on a real 8.5 m length electric bus at a constant shaft speed which is 900 rpm. The inlet and outlet temperatures of the coolant of the motor are measured experimentally. These experiments were performed on a real 8.5 m long electric bus. These values are shared with the authors of this paper by one of the bus manufacturers in Turkey which is using the considered synchronous motor on their busses. The inlet temperature of the motor coolant is measured at 49 °C during the experiment at constant shaft speed and the outlet temperature is measured at 55.9 °C. Table **3** shows the comparison of both the experimental and our model of the outlet temperature of the coolant when its inlet temperature is 49 °C. As can be seen, with the developed model only a 4 % error is achieved with the experiment.

Table 3: The coolant outlet temperature comparison between the experiment and the developed model.

	Experimental	Developed Model	Error
Coolant Inlet Temperature [°C]	49	49	**4.03**
Coolant Outlet Temperature [°C]	55.9	53.65	

5. Taguchi Method for Present Problem

For the optimization of the cooling system of the PMSM, the Taguchi method is applied. The orthogonal arrays and signal-to-noise ratio (S/N) are the mathematical tools that are used in this method. To perform the Taguchi method, the aim of the study and the target of the problem should be specified, the parameters should be determined, and the orthogonal array should be selected which is L16 in our case due to the 5 parameters with 4 different values, and finally, the noise signal analyze should be performed. The S/N ratio can be divided into three categories [51]:

Smaller is better: $$\frac{S}{N} = -\log \frac{1}{n}(\Sigma y^2) \quad (8)$$

Nominal is better: $$\frac{S}{N} = -log \frac{1}{n}\left(\Sigma \frac{Y}{S^2 y}\right) \quad (9)$$

Larger is better: $$\frac{S}{N} = -\log \frac{1}{n}\left(\frac{1}{y^2}\right) \quad (10)$$

There are four main geometrical parameters to develop a cooling jacket such as; Mass flow rate of the coolant (A), Pipe diameter (B), Number of pipe turns (C), Type of coolant fluid (D), and Torque (E). The changes in the values for all factors are tabulated and given in Table **4**.

Table 4: Taguchi method taken parameters and values.

Parameters	Value
Mass flow rate of the coolant (A) (l/min)	20 - 30 - 40 - 50
Pipe diameter (B) (mm)	17.7 - 19.0 - 25.4 - 31.7
Number of pipe turns (C)	12 – 16 – 20 – 24
Type of coolant fluid (D)	EGW60/40–PGW60/40–EGW50/50-THER
Torque (E) (Nm)	500 – 1000 – 1500 - 2000

6. Results and Discussion

As mentioned, due to the limited studies that are focusing on the cooling strategy of the motor, this study is focused on the cooling system of the considered PMSM. Thus, the results of the optimization of the cooling system of the 250 kW PMSM are found and necessary discussions are performed based on the analysis. As illustrated in Table **4**, five main parameters with four different values are taken into account for the optimization system of the motor. As can be seen, 4 of these parameters except torque are the main parameters that should be taken into account as an optimization parameter. The torque parameter is added as one of another parameters even though it is known that it will change along the driving cycle. But the bus manufacturers need this value due to the regulations that should mention the torque values for the driving cycles such as European driving cycle, American driving cycle, etc. Thus, torque is added as another parameter to the study.

Due to 5 parameters with 4 different values, L16 Taguchi orthogonal array is implemented (L16 (4^5); Factors: 5, Runs:16) for the Taguchi analysis. The experimental plan is used by considering Table **5**. As seen in Table **5**, the cooling water outlet temperature and the winding temperature for each run are found by using Minitab software. Based on these results, optimization is performed for the best cooling strategy for the motor. The effect of these parameters on the temperature is studied in this section and plotted in Fig. (**4**).

The runs of L16 array results are given in Fig. (**4**). The first curve on the left side of the figure shows that due to the increase in the mass flow rate of the refrigerant, the winding temperature decreases to reach the optimum value when the mass flow rate (A) is 50 l/min. The second parameter is the pipe diameter; the best diameter is the lowest one which is 17.7 mm. The third curve is related to the parameter (C) which is the number of pipe turns. The results showed that 20 turns are expected to be the best value. The fourth curve refers to the coolant type, EGW 50/50 is the best coolant type. The last curve in Fig. (**4**) shows the effect of the torque, this curve illustrates that 2000 Nm is the best optimum value at which the motor achieves the best efficiency.

Table 5: The plan of L16 orthogonal array and cooling water / winding temperatures.

Runs	Mass Flow Rate of the Coolant (A) (l/min)	Pipe Diameter (B) (mm)	Number of Pipe Turns (C)	Type of Coolant Fluid (D)	Torque (E)	Cooling Water Outlet Temp (°C)	Winding Temp (°C)
1.	20	17.7	12	EGW60/40	500	57.89	122.71
2.	20	19	16	PGW60/40	1000	57.31	104.1
3.	20	25.4	20	EGW50/50	1500	55.64	88.12
4.	20	31.7	24	THER	2000	50.4	97.85
5.	30	17.7	16	EGW50/50	2000	57.45	80.79
6.	30	19	12	THER	1500	56.75	104.42
7.	30	25.4	24	EGW60/40	1000	54.55	96.28
8.	30	31.7	20	PGW60/40	500	54.07	120.51
9.	40	17.7	20	THER	1000	57.75	103.74
10.	40	19	24	EGW50/50	500	54.31	114.01
11.	40	25.4	12	PGW60/40	2000	53.24	91.07
12.	40	31.7	16	EGW60/40	1500	53.84	86.14
13.	50	17.7	24	PGW60/40	1500	54.01	82.36
14.	50	19	20	EGW60/40	2000	54.86	77.22
15.	50	25.4	16	THER	500	55.39	122.61
16.	50	31.7	12	EGW50/50	1000	53.01	96.89

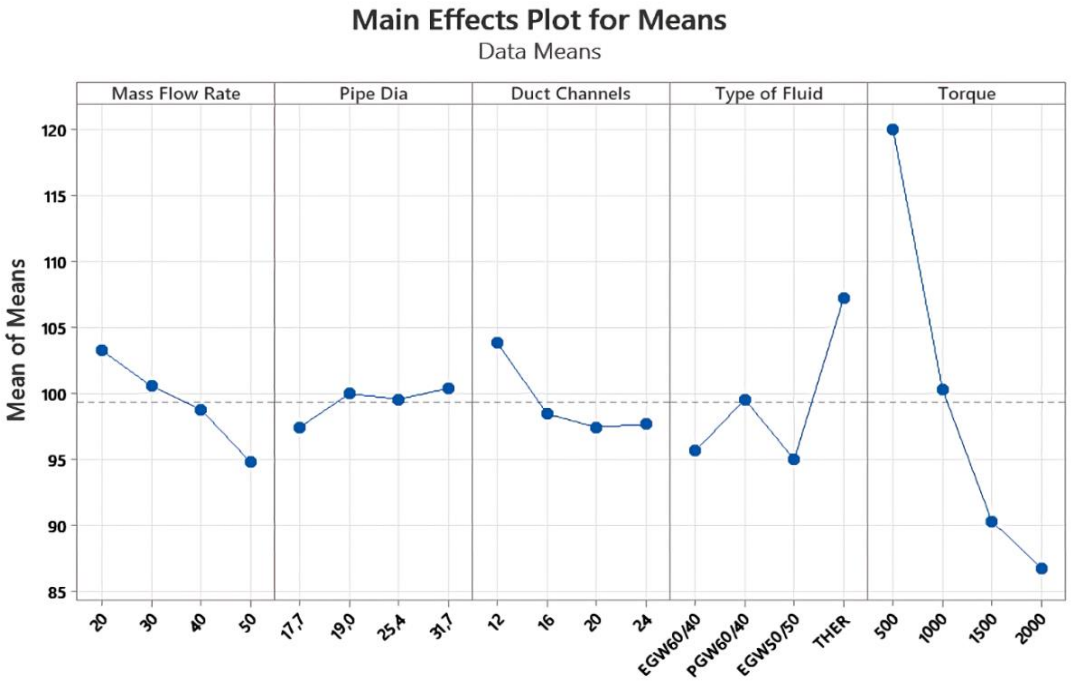

Figure 4: The plot of the main effect per level for means.

The response table for the S/N ratio is given in Table **6**. The maximum and minimum S/N ratios for all parameters are used to obtain the delta values. As seen from this table, parameter 5 (torque) is the most effective parameter for the performance of the motor. For the other 4 parameters, which can be changed in the design of

the motor, the type of the coolant fluid and the mass flow rate of the coolant have a significant effect on the cooling strategy of the motor. On the other hand, parameter 2, which is the pipe diameter has the lowest effective parameter.

Table 6: Results of the means.

Level	Mass Flow Rate (A)	Pipe Diameter (B)	Number of Turns (C)	Type of Fluid (D)	Torque (E)
1.	103.9	97.4	103.78	95.59	119.96
2.	100.5	99.94	98.41	99.51	100.25
3.	98.74	99.52	97.40	94.95	90.26
4.	94.77	100.35	97,62	107.16	86.73
Delta	8.42	2.94	6.38	12.20	33.23
Rank	3	5	4	2	1

As seen in Table **7**, the A4B1C3D3E4 (mass flow rate of coolant = 50 l/min, pipe dimeter=17.7 mm, 20 pipe turn, EGW50/50, and 2000 Nm torque) gives the best cooling strategy for reducing the winding temperature. Thus, the best design for the cooling of the motor is the A4B1C3D3E4 combination. The worst cooling design for the performed motor is A1B4C1D4E1. Based on these results, for the best design case, the coolant outlet temperature and the winding temperature are found as around 55 °C and 76.6 °C when the inlet coolant temperature is 49 °C, respectively. For the worst design case, the coolant outlet temperature and the winding temperatures are around 54.6 °C and 151 °C when the inlet coolant temperature is 49 °C, respectively. As can be seen clearly, there is a huge winding temperature difference between the best and the worst case.

Table 7: Coolant outlet and winding temperature of the best and worst case.

750 V 900 rpm	Coolant Inlet Temp (ºC)	Coolant Outlet Temp (ºC)	Winding Temp (ºC)
Current design	49	53.65	96.60
A4B1C3D3E4 (best case)		55.09	76.64
A1B4C1D4E1 (worst case)		54.62	151.05

Fig. (**5**) shows the thermal distribution of these three models: current (A1B3C1D1E4), worst (A1B4C1D4E1), and best (A4B1C3D3E4) models. As can be seen, to analyze the difference between current, worst, and best models, the legend of the temperature distribution is fixed for all cases from 50 °C to 180 °C. As seen in Fig. (**5a**), which illustrates the current design temperature distribution, the average temperature of the whole motor is around 80 °C while the winding temperature is at 96.6 °C as given in Table **7**. On the other hand, the average temperature of the motor for the worst (Fig. **5b**) and the best (Fig. **5c**) cases is around 140 °C and 75 °C, while the winding temperature is at 151.0 °C and 76.64 °C, respectively. The results showed us that, the increase in winding temperature directly affects the total average temperature of the motor.

Fig. (**5**) and Fig. (**6**) illustrate the change of the temperature of the cooling outlet water and winding average temperature according to time, at three different models, (best, current, and worst case).

Fig. (**6**) shows the winding temperature increase by time in three different models (current, optimum, and worst model) the best model winding temperature reaches 76.6 °C as the maximum temperature, while in the current model, the temperature increases to 96.6 °C, and as can be seen from the graph at worst parameters the temperature can reach to 151 °C. The worst case reaches 100 °C suddenly, around 100 sec later. There is no doubt that this design will necessarily negatively affect the aging and efficient operation of the engine.

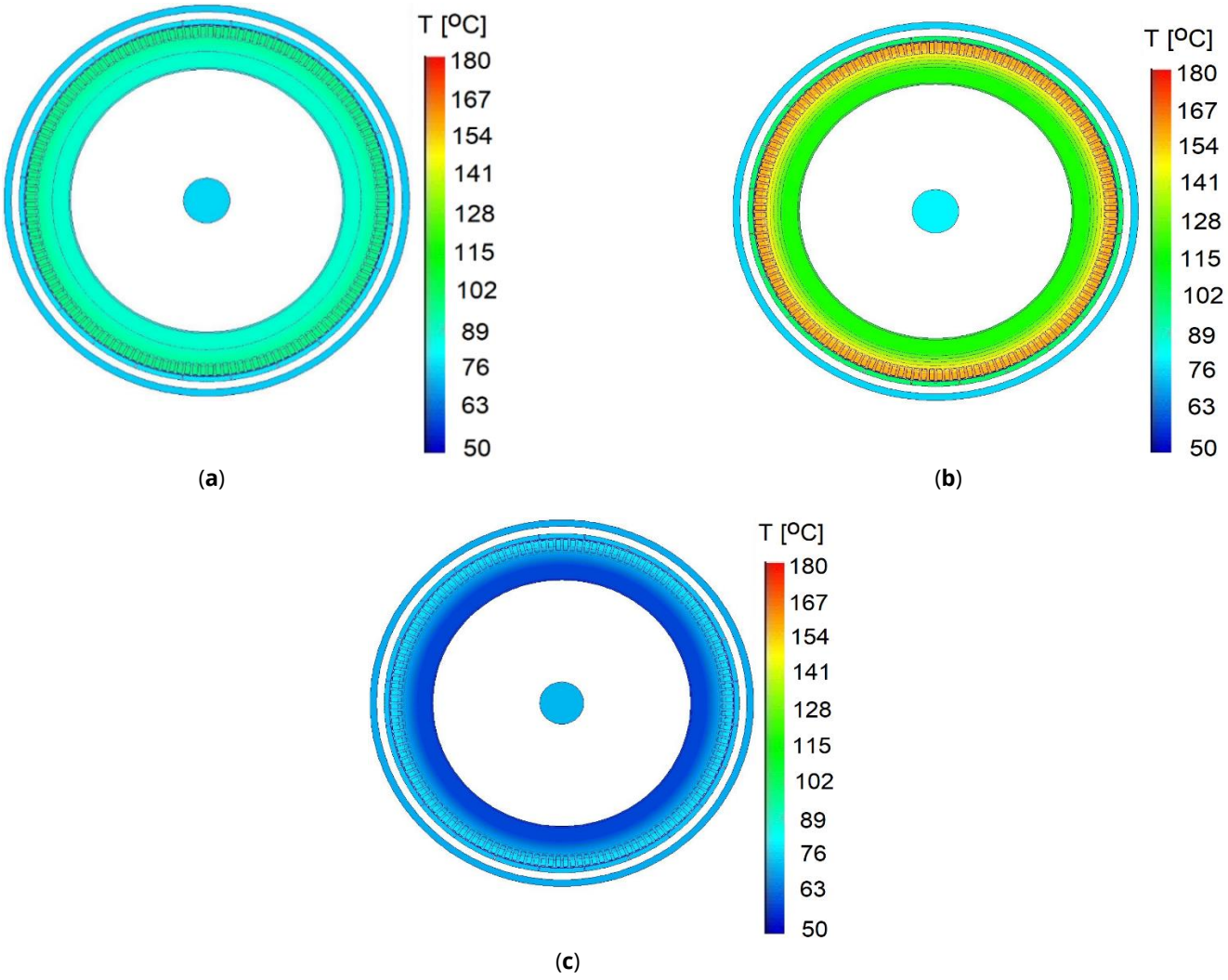

Figure 5: Thermal distribution comparison of the **a**) Current, **b**) Worst **c**) Best design.

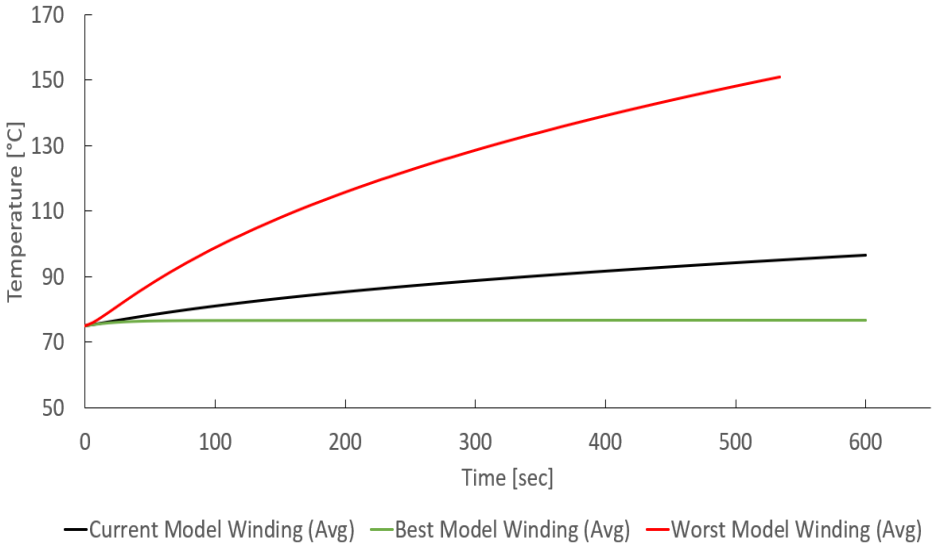

Figure 6: Comparison between current, worst, and optimum model temperatures of winding (avg).

The cooling jacket temperatures (Fig. **7**) reached about the same degree at the end. In this case, the earlier stages are more important because the cooling jacket temperature should be increased easily at the beginning.

This indicates that it absorbs heat faster. The best model reaches 55 °C rapidly and then the temperature curve stabilizes at 55.9 °C. Because of that, 55 °C is chosen as the reference temperature. The best model reaches 55 °C at 138 sec while the current model and worst model temperatures are respectively 50.94 °C and 82.86 °C. The optimum performance increases by 7.97 % compared to housing jacket outlet temperature at 138 sec. The optimum performance increases by 19.39 % compared to the winding temperature for the cooling jacket. This improvement results can be seen easily as shown in Fig. (**5**) and Fig. (**6**).

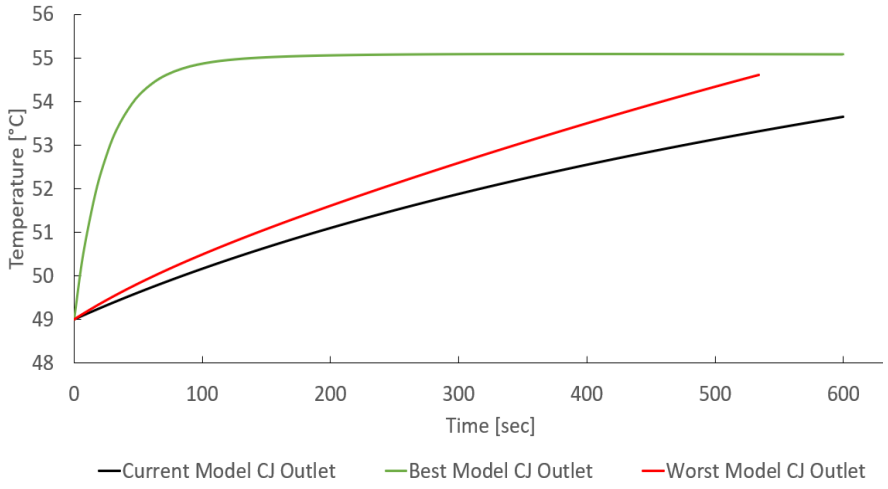

Figure 7: Comparison between current, worst, and optimum model temperatures of the cj outlet.

The cooling jacket temperatures reached about the same degree at the end. In this case, the earlier stages are more important because the cooling jacket temperature should be increased easily at the beginning. This indicates that it absorbs heat faster. The best model reaches 55 °C rapidly and then the temperature curve stabilizes at 55.9 °C. Because of that, 55 °C is chosen as the reference temperature. The best model reaches 55 °C at 138 sec while the current model and worst model temperatures are respectively 50.94 °C and 82.86 °C. The optimum performance increases by 7.97 % compared to housing jacket outlet temperature at 138 sec. The optimum performance increases by 19.39 % compared to the winding temperature for the cooling jacket. This improvement results can be seen easily as shown in Fig. (**6**) and Fig. (**7**).

7. Conclusions

In this study, thermal analysis of a 250 kW permanent magnet synchronous motor was taken into account. Firstly, the e-magnetic model of the motor is studied. Secondly, the thermal analysis is performed. To increase the efficiency of the motor, the cooling parameters of the motor are optimized. After the validation of the e-magnetic model and thermal model, design changes have been made to the coolant jacket to improve the cooling performance of the motor obtained in the analysis environment by applying the Taguchi method. The parameters such as mass flow rate: 50 l/min, pipe diameter: 17.7 mm, number of turns: 20, type of fluid: EGW 50/50, torque: 2000 Nm for the motor are found the best parameters for cooling the motor. By this method, the winding temperature of the PMSM decreased to 79°C from 98°C. The results showed that thermal efficiency can be increased by using the best design parameters 19.39 % compared with the current design with the changes in the cooling jacket design parameters.

Conflict of Interest

The authors declare that there is no conflict of interest.

Funding

The study received no financial support.

Nomenclature

B_d	Peak flux density value in the teeth
C	Thermal capacitance (unit: J/K)
Cp	Calorific capacity (unit: J/kg)
c_s	Is the specific heat (unit: J/kg K)
f	Supply frequency of the motor
l	Thickness of the layer (unit: m)
L_{sp}	Spire average length (unit: m)
M_{ds}	Teeth mass
S	Area of the layer (unit: m^2)
T	The temperature unit: (K)
T_{cu}	Copper temperature (unit: K)
V	Material volume (unit: m^3)
Ra	Material volume (unit: m^3)
q	Quality coefficient of meta sheets
ρ	The density (unit: kg/m^3)
λ	Thermal conductivity (unit: $Wm^{-1} K^{-1}$)

References

[1] European Commission. EU transport in figures - Statistical pocketbook. 2011. Available from: https://ec.europa.eu- /transport/facts-fundings/statistics/pocketbook-2011_en/ (accessed on 21 February 2021).

[2] Zhang Q, Tan L, Xu G. Evaluating transient performance of servo mechanisms by analysing stator current of PMSM. Mech Syst Signal Process. 2018; 101: 535–48. https://doi.org/10.1016/j.ymssp.2017.09.011

[3] Moosavi SS, Djerdir A, Amirat YA, Khaburi DA. Demagnetization fault diagnosis in permanent magnet synchronous motors: A review of the state-of-the-art. J Magn Magn Mater. 2015; 391: 203–12. https://doi.org/10.1016/j.jmmm.2015.04.062

[4] Staton D, Pickering S, Lampard D. Recent advancement in the thermal design of electric motors. Proceedings of the SMMA 2001 Fall Technical Conference "Emerging Technologies for Electric Motion Industry," Durham, North Carolina, USA: Oct. 3-5, 2001.

[5] Huang Z, Marquez F, Alakula M, Yuan J. Characterization and application of forced cooling channels for traction motors in HEVs. 2012 XXth International Conference on Electrical Machines, Marseille, France: IEEE; 2012, p. 1212–8. https://doi.org/10.1109/ICElMach.2012.6350030

[6] Kim M-S, Lee K-S, Um S. Numerical investigation and optimization of the thermal performance of a brushless DC motor. Intl J Heat Mass Transf. 2009; 52: 1589–99. https://doi.org/10.1016/j.ijheatmasstransfer.2008.07.040

[7] Lim DH, Kim SC. Thermal performance of oil spray cooling system for in-wheel motor in electric vehicles. Appl Therm Eng. 2014; 63: 577–87. https://doi.org/10.1016/j.applthermaleng.2013.11.057

[8] Zhang Y, Shen Y, Zhang W. Optimized design of the cooling system for and articulated dump truck's electric drive system, SAE Technical Paper 2010-01-0504, 2010. https://doi.org/10.4271/2010-01-0504

[9] Polikarpova M, Lindh PM, Tapia JA, Pyrhonen JJ. Application of potting material for a 100 kW radial flux PMSM. 2014 International Conference on Electrical Machines (ICEM), Berlin, Germany: IEEE; 2014, p. 2146–51. https://doi.org/10.1109/ICELMACH.2014.6960481

[10] Yang Y, Bilgin B, Kasprzak M, Nalakath S, Sadek H, Preindl M, *et al*. Thermal management of electric machines. IET Electr Syst Transp. 2017; 7: 104–16. https://doi.org/10.1049/iet-est.2015.0050

[11] Rehman Z, Seong K. Three-D numerical thermal analysis of electric motor with cooling jacket. Energies (Basel). 2018; 11: 1196–1073. https://doi.org/10.3390/en11010092

[12] Cavazzuti M, Gaspari G, Pasquale S, Stalio E. Thermal management of a Formula E electric motor: Analysis and optimization. Appl Therm Eng. 2019; 157: 113733. https://doi.org/10.1016/j.applthermaleng.2019.113733

[13] Zhang Y, Ruan J, Huang T, Yang X, Zhu H, Yang G. Calculation of temperature rise in air-cooled induction Motors through 3-D coupled electromagnetic fluid-dynamical and thermal finite- element analysis. IEEE Trans Magn. 2012; 48: 1047–50. https://doi.org/10.1109/TMAG.2011.2174433

[14] Lundmark ST, Acquaviva A, Bergqvist A. Coupled 3-D thermal and electromagnetic modelling of a liquid-cooled transverse flux traction motor. 2018 XIII International Conference on Electrical Machines (ICEM), Alexandroupoli, Greece: IEEE; 2018, p. 2640–6. https://doi.org/10.1109/ICELMACH.2018.8506835

[15] Aziz R, Atkinson GJ. Thermal model for permanent magnet synchronous machine. Int J Power Electr Drive Sys (IJPEDS). 2017; 8: 1903-12. https://doi.org/10.11591/ijpeds.v8.i4.pp1903-1912

[16] Demetriades GD, Karatsivos E, Agelidis V, Konstantinou G. A real-time thermal model of a permanent-magnet synchronous motor. IEEE Trans Power Electron. 2010; 25: 463–74. https://doi.org/10.1109/TPEL.2009.2027905

[17] Ponomarev P, Polikarpova M, Pyrhonen J. Thermal modeling of directly-oil-cooled permanent magnet synchronous machine. 2012 XXth International Conference on Electrical Machines, Marseille, France: IEEE; 2012, p. 1882–7. https://doi.org/10.1109/ICElMach.2012.6350138

[18] Tikadar A, Johnston D, Kumar N, Joshi Y, Kumar S. Comparison of electro-thermal performance of advanced cooling techniques for electric vehicle motors. Appl Therm Eng. 2020; 183: 116182. https://doi.org/10.1016/j.applthermaleng.2020.116182

[19] Fan J, Zhang C, Wang Z, Dong Y, Nino CE, Tariq AR, *et al*. Thermal analysis of permanent magnet motor for the electric vehicle application considering driving duty cycle. IEEE Trans Magn. 2010; 46: 2493–6. https://doi.org/10.1109/TMAG.2010.2042043

[20] Fang G, Yuan W, Yan Z, Sun Y, Tang Y. Thermal management integrated with three-dimensional heat pipes for air-cooled permanent magnet synchronous motor. Appl Therm Eng. 2019; 152: 594-604. https://doi.org/10.1016/j.applthermaleng.2019.02.120

[21] Sun Y, Zhang S, Yuan W, Tang Y, Li J, Tang K. Applicability study of the potting material-based thermal management strategy for permanent magnet synchronous motors. Appl Therm Eng. 2019; 149: 1370–8. https://doi.org/10.1016/j.applthermaleng.2018.12.141

[22] Cermak R, Pechanek R. Thermal study of permanent magnet direct drive wheel motor. Proceedings of the 2018 18th International Conference on Mechatronics - Mechatronika, ME 2018, 2018, p. 1–6.

[23] Chaieb M, Ben Hadj N, Kammoun JK, Neji R. Thermal modeling of permanent magnet motor with finite element method. 2014 15th International Conference on Sciences and Techniques of Automatic Control and Computer Engineering (STA), Hammamet, Tunisia: IEEE; 2014, p. 594–8. https://doi.org/10.1109/STA.2014.7086733

[24] Demetriades GD, Zelaya De La Parra H, Andersson E, Olsson H. A real-time thermal model of a permanent magnet synchronous motor based on geometrical measures. 2008 IEEE Power Electronics Specialists Conference, Rhodes, Greece: IEEE; 2008, p. 3061–7. https://doi.org/10.1109/PESC.2008.4592420

[25] Kazan FA, Bilgin O. Simulation of PMSM operating at different speeds and optimization of PI controller parameters. Mehmet Akif Ersoy Üniversitesi Uygulamalı Bilimler Dergisi 2020; 4: 86–105. https://doi.org/10.31200/makuubd.673400

[26] Jebahi R, Aloui H, Ayadi M. One-dimensional lumped-circuit for transient thermal study of an induction electric motor. Int J Electr Comput Eng (IJECE). 2017; 7: 1714-24. https://doi.org/10.11591/ijece.v7i4.pp1714-1724

[27] Kacenka A, Pop A-C, Vintiloiu I, Fodorean D. Lumped parameter thermal modeling of permanent magnet synchronous motor. 2019 Electric Vehicles International Conference (EV), Bucharest, Romania: IEEE; 2019, p. 1–6. https://doi.org/10.1109/EV.2019.8892937

[28] Kahrisangi MG, Isfahani AH, Vaez-Zadeh S, Sebdani MR. Line-start permanent magnet synchronous motors versus induction motors: A comparative study. Front Inf Technol Electron Eng. 2012; 7: 459–66. https://doi.org/10.1007/s11460-012-0217-8

[29] Kefalas TD, Kladas AG. Finite element transient thermal analysis of PMSM for aerospace applications. XXth International Conference on Electrical Machines, Marseille, France: IEEE; 2012, p. 2566–72. https://doi.org/10.1109/ICElMach.2012.6350246

[30] Kefalas TD, Kladas AG. Thermal investigation of permanent-magnet synchronous motor for aerospace applications. IEEE Trans Industr Electr. 2014; 61: 4404–11. https://doi.org/10.1109/TIE.2013.2278521

[31] Kim C, Lee K-S, Yook S-J. Effect of air-gap fans on cooling of windings in a large-capacity, high-speed induction motor. Appl Therm Eng. 2016; 100: 658–67. https://doi.org/10.1016/j.applthermaleng.2016.02.077

[32] Li GJ, Ojeda J, Hoang E, Gabsi M. Thermal-electromagnetic analysis of a fault-tolerant dual-star flux-switching permanent magnet motor for critical applications. IET Electr Power Appl. 2011; 5: 503-13. https://doi.org/10.1049/iet-epa.2010.0250

[33] Malumbres JA, Satrustegui M, Elosegui I, Ramos JC, Martínez-Iturralde M. Analysis of relevant aspects of thermal and hydraulic modeling of electric machines. Application in an open self ventilated machine. Appl Therm Eng. 2015; 75: 277–88. https://doi.org/10.1016/j.applthermaleng.2014.10.012

[34] Meenen J. Electric vehicle team porsche designing a cooling system for the AC24 electric motor. Massachusetts Technology Institute, 2010.

[35] Mutlu Y. Elektriklı araç motorunun sogutma sıstem tasarımı. Yuksek Lisans Tezi. Istanbul Teknik Universitesi; 2011.

[36] Putra N, Ariantara B. Electric motor thermal management system using L-shaped flat heat pipes. Appl Therm Eng. 2017; 126: 1156–63. https://doi.org/10.1016/j.applthermaleng.2017.01.090

[37] Rehman Z, Seong K. Three-D numerical thermal analysis of electric motor with cooling jacket. Energies (Basel). 2018; 11: 92. https://doi.org/10.3390/en11010092

[38] Satrústegui M, Martinez-Iturralde M, Ramos JC, Gonzalez P, Astarbe G, Elosegui I. Design criteria for water cooled systems of induction machines. Appl Therm Eng. 2017; 114: 1018–28. https://doi.org/10.1016/j.applthermaleng.2016.12.031

[39] Staton DA, Popescu M, Hawkins D, Boglietti A, Cavagnino A. Influence of different end region cooling arrangements on end-winding heat transfer coefficients in electrical machines. 2010 IEEE Energy Conversion Congress and Exposition, Atlanta, GA, USA: IEEE; 2010, p. 1298–305. https://doi.org/10.1109/ECCE.2010.5617810

[40] Tauseef MG, Chao S. Thermal analysis of PMSM stator using ANSYS. Master Thesis. Technische Universitat Darmstadt; 2014.

[41] Ustun O, Cakan M, Tuncay RN, Mokukcu MS, Kivanc OC, Mutlu Y, *et al*. Design and manufacture of electric powertrain and its cooling system for ITU EV project. 2014 International Conference on Electrical Machines (ICEM), Berlin, Germany: IEEE; 2014, p. 730–5. https://doi.org/10.1109/ICELMACH.2014.6960262

[42] Üstün Ö, Tuncay RN, Mökükcu MS, Kivanç ÖC, Tosun G, Gökçe C, *et al*. An integrated approach for the development of an electric vehicle powertrain: Design, analysis, and implementation. Turk J Electr Eng Comput Sci. 2018; 26: 1541–54. https://doi.org/10.3906/elk-1701-136

[43] Wang S, Li Y, Li Y-Z, Wang J, Xiao X, Guo W. Transient cooling effect analyses for a permanent-magnet synchronous motor with phase-change-material packaging. Appl Therm Eng. 2016; 109: 251–60. https://doi.org/10.1016/j.applthermaleng.2016.08.036

[44] Ragazzo P. Advanced e-machine design using open-access scripting languages with Motor-CAD solving engine. Master's Thesis. Polıtecnıco Dı Torıno; 2020. Available from https://webthesis.biblio.polito.it/14009/1/tesi.pdf

[45] Xia ZP, Zhou CQ, Shen D, Ni HJ, Yuan YN, Ping L. Study on the cooling system of super-capacitors for a hybrid electric vehicle. Appl Mech Mater. 2014; 492: 37–42. https://doi.org/10.4028/www.scientific.net/AMM.492.37

[46] Xie Y, Wang Y. 3D temperature field analysis of the induction motors with broken bar fault. Appl Therm Eng. 2014; 66: 25–34. https://doi.org/10.1016/j.applthermaleng.2014.02.008

[47] Sun Y, Zhang S, Yuan W, Tang Y, Li J, Tang K. Applicability study of the potting material-based thermal management strategy for permanent magnet synchronous motors. Appl Therm Eng. 2019; 149: 1370–8. https://doi.org/10.1016/j.applthermaleng.2018.12.141

[48] TM4 SUMO^{TM} HD. https://www.danatm4.com/products/systems/sumo-hd/ (June 28, 2022).

[49] Touhami S, Bertin Y, Lefèvre Y, Llibre JF, Henaux C, Fenux M. Lumped parameter thermal model of permanent magnet synchronous machines. Electrimacs, Toulouse, France: University of Toulouse; 2017.

[50] Fakhfakh MA. Thermal analysis of a permanent magnet synchronous motor for electric vehicles. J Asian Electr Veh. 2008; 6: 1145–51. https://doi.org/10.4130/jaev.6.1145

[51] Gediz Ilis G, Demir H. A new adsorbent bed design: Optimization of geometric parameters and metal additive for the performance improvement. Appl Therm Eng. 2019; 162: 114270. https://doi.org/10.1016/j.applthermaleng.2019.114270